Journal of Catalysis 269 (2010) 388–396

Contents lists available at ScienceDirect

Journal of Catalysis

journal homepage: www.elsevier.com/locate/jcat

Investigations on the properties of ceria–zirconia-supported Ni and Rh catalysts and their performance in acetic acid steam reforming

Ekaterini Ch. Vagia, Angeliki A. Lemonidou *

Department of Chemical Engineering, Aristotle University of Thessaloniki and Chemical Process Engineering Research Institute, University Campus, GR-54124 Thessaloniki, Greece

ARTICLE INFO

Article history:
Received 19 November 2009
Accepted 24 November 2009
Available online 24 December 2009

Keywords:
Hydrogen production
Steam reforming
Acetic acid
CeO_2–ZrO_2
Ni catalyst
Rh catalyst
Oxygen storage capacity
Isotopic oxygen exchange

ABSTRACT

The production of hydrogen via steam reforming of acetic acid was examined over Ni and Rh supported on a CeO_2–ZrO_2-mixed oxide. The catalysts were tested at 550–650–750 °C using steam/carbon = 3. Steam reforming, water gas shift, and decarboxylation are the main reactions taking place over the support alone. In parallel, dehydrogenation leads to the formation of carbon deposits on the surface of the mixed oxide. The addition of the metals enables the reforming reactions to proceed with high rates producing hydrogen yields close to thermodynamic equilibrium even at 650 °C. The oxygen exchange reactions are enhanced leading to much lower coke deposition. The nature of the metal affects not only the quantity but also the quality and the location of the carbon deposits, as evidenced from temperature-programing oxidation tests. The synergy of the support and metal is the key factor for the low coke deposition, which is even lower for the Rh catalyst.

1. Introduction

Hydrogen has great potential as an environmentally clean energy fuel. Since hydrogen does not exist on earth as a gas, it must be obtained from other compounds such as water, biomass, and natural gas. The two most common methods for producing hydrogen are steam reforming and electrolysis. Nowadays, a large amount of hydrogen that is commercially used for ammonia production and refining processes is produced from fossil fuels such as natural gas, naphtha, heavy oil, and coal via steam reforming and partial oxidation processes [1].

The depletion of currently used sources of hydrogen and the substantial amounts of CO_2 emitted to the atmosphere during the process steps associated with its production lead to apprehension. Biomass has been proposed as an alternative feedstock for hydrogen production not only because it is renewable but also because it is a CO_2 neutral energy source.

Hydrogen can be produced from biomass mainly via two thermochemical processes, gasification [2,3] and flash pyrolysis [4–6] followed by steam reforming of the pyrolysis oil. The pyrolysis oil, known as bio-oil, is a complex mixture of acids, alcohols, aldehydes, esters, ketones, sugars, phenols, guaiacols, syringols, furans, and multifunctional compounds [7]. Steam reforming can be used to convert the entire bio-oil or each of the oil fractions, the hydrophilic light fraction and the hydrophobic heavier fraction, to hydrogen-rich stream.

Thermodynamic calculations of steam and autothermal reforming of particular model compounds of bio-oil, acetic acid, ethylene glycol, and acetone showed that the oxygenates in the presence of steam are easily converted to hydrogen-rich mixtures achieving maximum hydrogen yield (80–90%) at 625 °C without any coke formation for operation under atmospheric pressure and steam/carbon > 1 [8,9].

Several studies have been reported for acetic acid steam reforming [10–20]. The influence of Ni and noble metals and the type of the support (Al_2O_3, La_2O_3/Al_2O_3, and MgO/Al_2O_3) on acetic acid steam reforming has been persistently studied. The main conclusions point to the crucial effect of the metal type and support on the hydrogen selectivity and yield and the high tendency of the thermally unstable oxygenates to decompose forming carbonaceous deposits which limit their large scale application especially in conventional fixed bed reactors [12].

Catalytic materials based on CeO_2–ZrO_2 have been demonstrated to be active in methane steam reforming with stable behavior, high methane conversions, and hydrogen yields approaching those of thermodynamic equilibrium. Above all, the ability of these catalytic materials to resist carbon deposition renders them attractive in reforming reactions. Partial oxidation, CO_2 reforming and steam reforming of methane using Ni and Pt over CeO_2–ZrO_2, CeO_2, and ZrO_2 have been widely examined in the literature

* Corresponding author. Fax: +30 2310 996184.
E-mail address: alemonidou@cheng.auth.gr (A.A. Lemonidou).

0021-9517/$ - see front matter © 2009 Elsevier Inc. All rights reserved.
doi:10.1016/j.jcat.2009.11.024

[21–28]. In addition, the ceria–zirconia system has been investigated in phenol and ethanol reforming [29–36]. Despite the promising results of these materials concerning their high activity in combination with coke resistance in reforming reactions, their application in steam reforming of bio-oil and its components has received less attention [37,38].

Our recent publication [39], concerning acetic acid and acetone steam reforming over Ni and Rh supported on Ca–Al-mixed oxides, showed that hydrogen yield depends on the metal type and loading and the ratio of CaO to Al_2O_3. Both Ni- and Rh-containing catalysts were proved to be very effective in converting acetic acid and acetone to hydrogen with relatively low carbonaceous depositions.

The aim of the present work is to investigate acetic acid steam reforming over ceria–zirconia-mixed oxide-supported catalysts. The influence of active metal (Ni and Rh) on hydrogen yield, and the synergetic action of the support and metal on the nature and the quantity of carbon deposits are investigated using continuous flow experiments of acetic acid reforming and thermo-programing techniques.

2. Experimental

2.1. Catalyst preparation

The wet impregnation method was applied for the catalysts' preparation. Cerium-doped zirconium hydroxide provided by Mel Chemicals (XZO802) was calcined at 800 °C for 4 h. The calcined material with a composition CeO_2/ZrO_2 = 15/85(wt) was used as the support. $Ni(NO_3)_2{\cdot}6H_2O$ and $RhCl_3{\cdot}3H_2O$ were the precursors for the nickel (5 wt%) and rhodium (0.5 wt%) metals, respectively. The aqueous solution of the precursors was mixed with the support particles and stirred for 1 h at 70 °C. The solvent was removed via evaporation under mild vacuum conditions and the samples were dried afterward overnight at 120 °C. The catalytic materials were calcined in air flow at 400 °C for 2 h. Before the reforming experiments, the catalysts were reduced at 750 °C for 1 h in 25% H_2/He flow.

The catalytic materials are referred to as *z*Me/Ce–Zr (where *z* is the metal wt% and Me is Ni or Rh) for samples supported on CeO_2–ZrO_2.

2.2. Catalyst characterization

The surface area of the prepared materials was measured by N_2 adsorption at 77 K, using the multipoint BET analysis method with an Autosorb-1 Quantachrome flow apparatus. The samples were dehydrated in vacuum at 250 °C overnight, before surface area measurements. X-ray diffraction (XRD) patterns were obtained using a Siemens D500 diffractometer, with Cu Kα radiation.

NH_3 temperature-programed desorption (TPD-NH_3) was used to determine the acidic properties of the catalysts. The experiments were performed in a gas flow system using a U-tube reactor connected online with a quadrupole mass analyzer (Omnistar, Balzers). The catalysts (200 mg) were pretreated at 650 °C for 0.5 h and then cooled to 100 °C under He flow. The pretreated samples were saturated with 5% NH_3/He for 1 h at 100 °C, with subsequent flushing with He at 100 °C for 1 h to remove the physisorbed ammonia. TPD analysis was carried out from 100 to 700 °C at a heating rate of 10 °C/min. Quantitative analysis of the desorbed ammonia was based on (*m*/*z*) 15.

Temperature-programed reduction (TPR) experiments were performed in the same setup with the TPD NH_3 experiments. The catalyst sample (200 mg) was placed in a U-shaped quartz reactor and pretreated for 0.5 h at 650 °C in flowing 15% O_2/He followed by cooling at room temperature in He flow. The temperature was then raised from room temperature to 900 °C at a rate of 10 °C/min in a 5% H_2/He flow (30 cm^3/min).

The metal dispersion was measured with H_2 temperature-programed desorption (TPD-H_2). Using the same flow system as mentioned above the catalysts (300 mg) were treated at 600 °C for 1 h under 20% O_2/He flow, then cooled to 300 °C, and then reduced with 20% H_2/He for 1 h at the reduction temperature of the metal (470 °C for Ni and 300 °C for Rh). The reduced sample was heated to 500 °C in He flow to desorb any H_2 than might have been spilled over the support and then cooled down to room temperature. A flow of 5% H_2/He was applied for 30 min at room temperature followed by He flow for another 30 min. The TPD analysis was carried out from room temperature to 700 °C at a heating rate of 10 °C/min.

For the measurements of the oxygen storage capacity (OSC) of the Ce–Zr-mixed oxide catalysts the sample (50 mg) was first pretreated at 750 °C for 0.5 h under He flow. Injection of pulses of H_2 every 100sec, at 750 °C, was applied up to a maximum reduction of the sample (25 pulses). The OSC was also measured using pre-reduced samples at 750 °C for 1 h under H_2 flow to simulate the conditions as in catalytic-reforming experiments (Section 2.4). The amount of μmol of O_2/g of catalyst, calculated according to the H_2 consumption of the first pulse, is considered as the active oxygen of the catalyst and represents the OSC. The sum of the μmol O_2/g of catalyst of the first 10 pulses presented as OSCC characterizes the total amount of oxygen available in oxide [40].

The oxygen surface mobility was examined with the oxygen isotopic exchange experiments. The materials (300 mg) were first reduced at the specific reduction temperature of the metal (300 °C for Rh and 470 °C for Ni) to ensure that the support remains in oxidized form. Then, they were cooled under He flow to room temperature before the reaction. The isotopic exchange of oxygen (2% $^{18}O_2$/He) was temperature programed from 50 to 750 °C with a rate of 15 °C/min. The ratios *m*/*z* 32, 34, and 36 were monitored for the $^{16}O_2$, $^{16}O^{18}O$, and $^{18}O_2$, respectively.

The used catalysts were transferred to a CHN stoichiometric analyzer LECO 800, for the measurement of the solid carbon deposited on the catalyst. The oxidation temperature of the solid carbon was also measured in a thermogravimetric unit (STD2960 TA Instruments), by subjecting the catalyst in temperature-programed oxidation with a rate of 10 °C/min up to 1000 °C, under air flow. The morphology of the carbon deposits was examined by scanning electron microscopy (SEM) on a JEOL 6300 microscope.

2.3. Catalytic testing

The experiments were performed at atmospheric pressure in a laboratory unit equipped with a mass flow-controlled system for gases admission, a fixed bed quartz reactor, and an online gas chromatograph. An HPLC pump (Gilson 350) was used for the feeding of the liquid reactants (a mixture of acetic acid and water) to the reactor through a preheater. The fixed bed reactor was heated electrically by a tubular furnace, with three independently controlled temperature zones. The temperature in the middle of the catalytic bed was measured with a coaxial thermocouple. The hot gases exiting the reactor were cooled to condense the liquid products and the unconverted reactants. The gas phase products were analyzed with an online gas chromatograph (Varian 3700) equipped with TCD. To separate the gaseous products, two columns were used: Porapak Q for CO_2, C_2H_4, C_2H_6, and higher hydrocarbons and MS 5A for H_2, O_2, CO, and CH_4. The liquid products were analyzed offline in gas chromatograph (Varian 3300) equipped with FID using an HP-FFAP column.

The experiments were performed using a steam to carbon molar ratio of 3 in a temperature range from 550 to 750 °C at atmospheric pressure. The catalyst (50 mg) diluted with quartz particles (100 mg) was loaded in the quartz reactor. The inlet flow of the liquid mixture was set at 0.1 cm^3/min. Helium was used as diluent with a flow of l00 cm^3/min. The gas hourly space velocity G_CHSV (defined as the volume of gas C1-equivalent species in the feed at standard temperature and pressure per unit volume of catalyst per hour) was 34,500 h^{-1}.

The terms conversion and product yield used to describe the catalytic results in reforming the bio-oil components are presented in detail in our previous publication [39].

3. Results and discussion

3.1. Characterization of the catalysts

The catalysts prepared and their properties are compiled in Table 1. The surface area of the CeO_2–ZrO_2 support is not affected by the addition of the metals and the sequential calcination as shown from the values tabulated. The three samples have surface areas slightly higher than 40 m^2/g. The diffractogram of the bare support shows sharp peaks which are attributed to the mixed crystalline tetragonal phase of $Zr_{0.84}Ce_{0.16}O_2$. Both Ni and Rh catalysts show the same characteristic peaks of the mixed ceria–zirconia phase. In addition, the NiO crystal phase appears with the 5Ni/Ce–Zr sample as expected, while no peaks of Rh are detected due to the much lower metal loading.

3.1.1. Acidity (TPD-NH_3)

Temperature-programed desorption of ammonia is one of the typical methods for the determination of the acidity of solid materials. Fig. 1 presents the profiles of the ammonia desorbed from the samples as a function of temperature. The maximum of the ammonia desorbed is located at 170–200 °C with the bare support and the Rh catalysts, while it shifts to 250 °C with the Ni catalyst. The quantitative results expressed as the mmol of NH_3 desorbed per weight of the sample are shown in Table 1. A difference in the acidity is observed with the noble metal catalyst. The addition of the noble metal almost doubles the number of acidic sites compared to that of the support. This can be attributed to the type of the precursor ($Rh(Cl)_3$) used for the impregnation of the metal [41]. Examination of the catalyst with TEM EDS detector confirmed the presence of residual chlorine (not shown). On the other hand, the addition of nickel does not affect the number of acidic sites of the support but only slightly affects their ability to retain stronger ammonia as it is clear from Fig. 1 in agreement with the reported data [42].

3.1.2. Temperature-programed reduction (TPR)

According to the literature data, CeO_2 is reduced at two distinct temperatures of about 500 and 750–800 °C [43]. The first peak is attributed to the reduction of surface oxygen while the second peak is attributed to the reduction of bulk oxygen. On the other hand, ZrO_2 does not show any reduction peak.

Table 1
Physicochemical characteristics of the catalysts.

Sample	Ce–Zr	5Ni/Ce–Zr	0.5Rh/Ce–Zr
Metal, wt%	–	5	0.5
Support	CeO_2–ZrO_2	CeO_2–ZrO_2	CeO_2–ZrO_2
Surface area, m^2/g	41.8	43.1	43
Crystal phases	$Zr_{0.84}Ce_{0.16}O_2$	$Zr_{0.84}Ce_{0.16}O_2$, NiO	$Zr_{0.84}Ce_{0.16}O_2$
mmol NH_3/g catalyst	0.09	0.08	0.16
% Dispersion	–	0.72	12

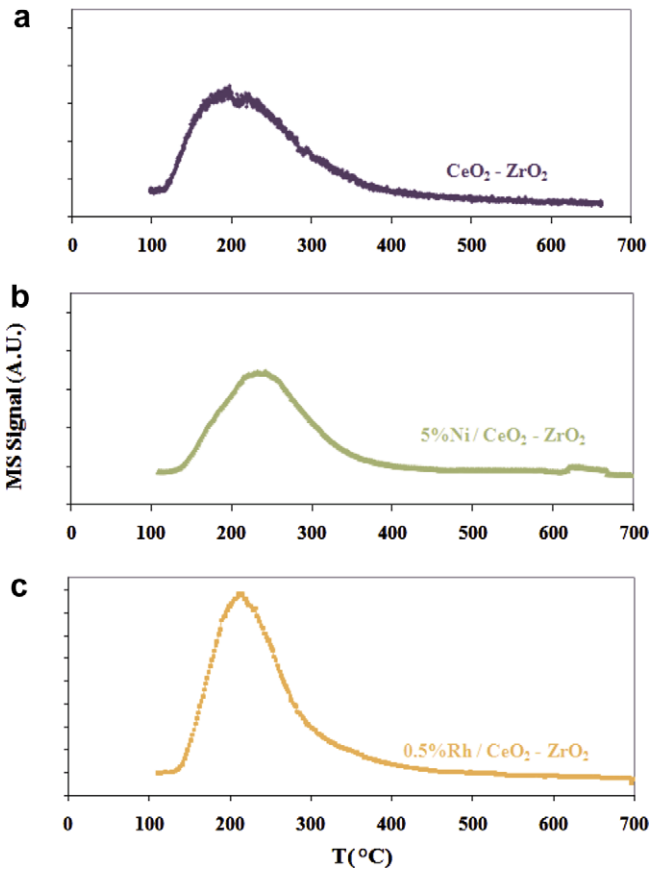

Fig. 1. Temperature-programed desorption of ammonia at (a) CeO_2–ZrO_2, (b) 5Ni/Ce–Zr, and (c) 0.5Rh/Ce–Zr.

Fig. 2a illustrates the temperature-programed reduction profile of CeO_2–ZrO_2-mixed oxide. The two very broad peaks centered at 450 and 675 °C are quite predictable and in agreement with the literature [43,44]. The lower temperature of CeO_2 reduction can be attributed to the high ZrO_2 loading of the mixed oxide as it is well known that the increasing of ZrO_2 content makes the reduction of bulk oxygen in Ce–Zr easier [43].

Fig. 2b depicts the reduction profile of the 5% Ni/CeO_2–ZrO_2 catalyst. NiO and part of CeO_2 (most probably surface oxygen species) seem to be reduced in the same temperature range (peak with maximum at 500 °C) while further reduction of the support continues up to 800 °C.

The profile of 0.5Rh/Ce–Zr catalyst is also presented in Fig. 2c. A peak at ca 100 °C is the characteristic of Rh reduction while a broad peak extended from 400 to 800 °C is ascribed to the support reduction. Quantitation of the results showed that the metals after the hydrogen treatment are fully reduced to metallic state while the support still contains significant amounts of oxygen (Table 2). Important to notice is that the extent of CeO_2 reduction depends on the presence of metals. The addition of 0.5% Rh to ceria increases the extent of its complete reduction from 53.7% to 66.3%.

3.1.3. Metal dispersion (TPD-H_2)

Ceria is well known as a support that improves the dispersion of metals [45] and especially that of noble metals [46]. The metal dispersion of the present catalytic materials was calculated based on the results of the temperature-programed hydrogen desorption.

Nickel catalyst exhibits a low dispersion, about 0.72%, most probably due to the strong interaction of nickel with the support

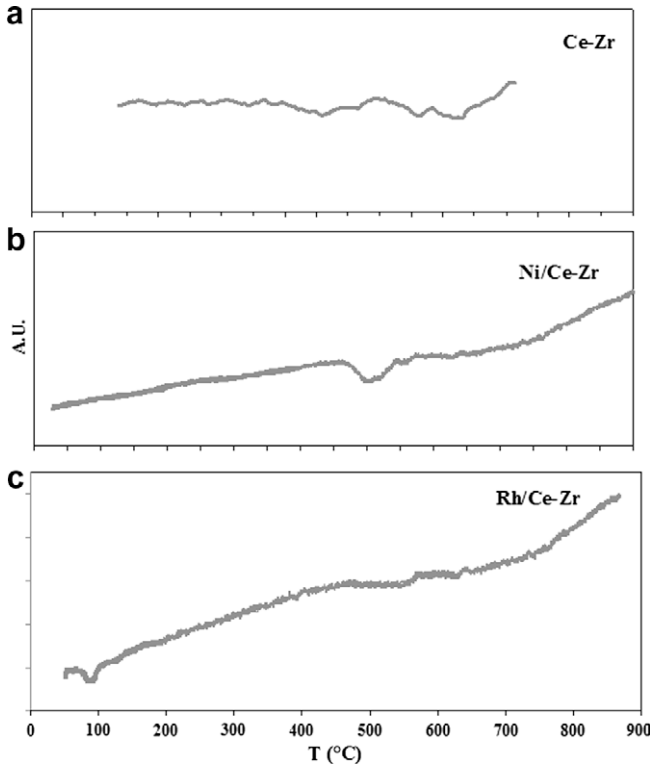

Fig. 2. Temperature-programed reduction profile of CeO_2–ZrO_2-supported catalysts.

Table 2
Extent of reduction of the metals and the support after temperature-programed reduction.

	Ce–Zr	5Ni/Ce–Zr	0.5Rh/Ce–Zr
Me^0, %	–	100	100
Up to 550 °C peak, %	10.2[a]	4.1	5.3
Over 550 °C peak, %	43.5	51.5	61

[a] The numbers appeared in the last two series refer to the % of ceria that has been reduced from +4 to 0.

[48,47]. A much higher dispersion ca. 12% is calculated with Rh catalyst [48].

3.2. Activity measurements in acetic acid reforming

The performance of the bare ceria–zirconia and that of the quartz loaded reactor at 750 °C are presented in Table 3. The activity of the support alone is around 30%, slightly higher than that obtained with the same reactor loaded with inert quartz. However, the distribution of the products is not similar, implying different extent of the reaction pathways. Over the ceria–zirconia sample the products are formed via the main routes of combined steam reforming and water gas shift (1), decarboxylation (2), and decomposition reactions (3). Methane formed via the decarboxylation reaction maybe further reformed producing hydrogen and COx. The molar ratio of H_2/CO in the product stream is around 3 implying that steam reforming rather than the simple decomposition (3) proceeds over the support. Decomposition of acetic acid would lead to a ratio of 1.

$$CH_3COOH + 2H_2O \rightarrow 2CO_2 + 4H_2 \quad (1)$$

$$CH_3COOH \rightarrow CH_4 + CO_2 \quad (2)$$

$$CH_3COOH \rightarrow 2CO + 2H_2 \quad (3)$$

The most important difference between the inert quartz and the ceria–zirconia support lies to the formation of substantial amounts of C2 hydrocarbons and especially of ethylene (yield 2.3%) in the presence of the latter.

Fig. 3a and b illustrates the conversion of acetic acid and product yields attained with the two catalysts containing Ni and Rh. The tests were performed at temperatures 550, 650, and 750 °C using H_2O to C ratio of 3 and space velocity based on carbon atoms

Table 3
Steam reforming of acetic acid over bare CeO_2–ZrO_2 support in comparison with thermal results (quartz) – conversion of acetic acid and product yield.

Sample	CeO_2–ZrO_2	Quartz
H_2O/C (molar ratio)	3	3
Temperature, °C	750	750
Weight of sample, g	0.05	0.05
Residence time τ, ms	4.5	4.5
Conversion, %	30	23
Product yield, %		
H_2	11.2	14.0
CO	6.4	9.5
CO_2	15.3	9.5
CH_4	5.4	3.5
Acetone	0.3	0.1
Ethane	0.3	–
Ethylene	2.3	–

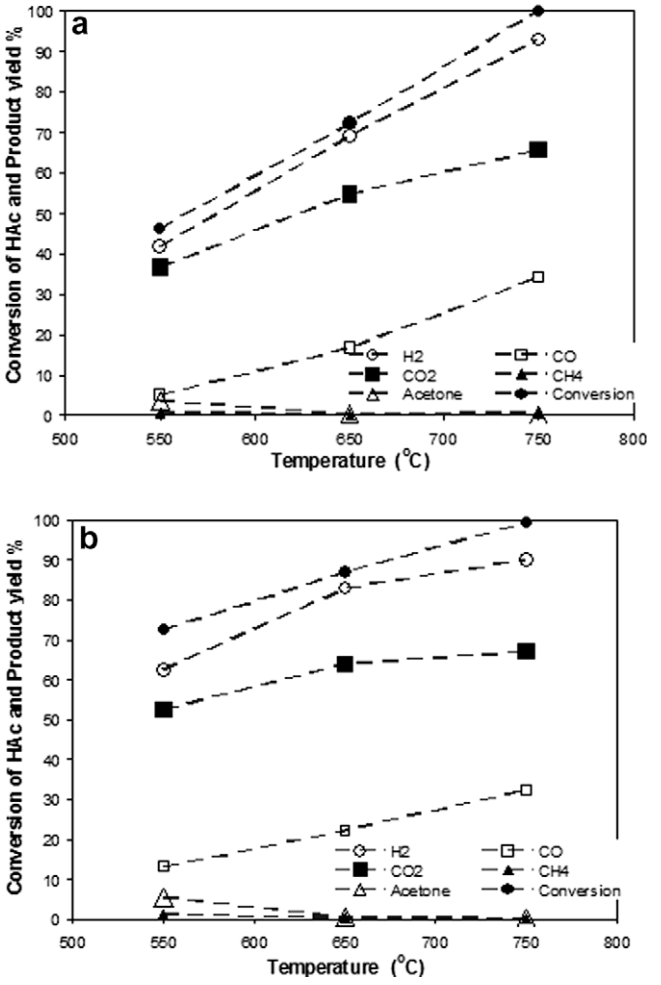

Fig. 3. Steam reforming of acetic acid over (a) Ni and (b) Rh catalysts supported on ceria–zirconia. Effect of temperature on the acetic acid conversion and product yields (steam/carbon = 3).

34,500 h^{-1}. It is obvious from Fig. 3 that the addition of the metal enables the reforming reactions to prevail as revealed from the high values of hydrogen yield which approach those of thermodynamic equilibrium at temperatures 650 and 750 °C [8]. The high yield of carbon dioxide indicates the contribution of water gas shift reaction at a high extent. The dominance of carbon oxides and hydrogen at 750 and 650 °C makes clear that the main reactions are that of reforming and water gas shift. Other intermediates formed are sequentially fully steam reformed. However, at the lowest temperature used 550 °C, the formation of low amounts of acetone and methane suggests that the ketonization (4) and decarboxylation (2) reactions also proceed with much lower rates

$$2CH_3COOH \rightarrow CH_3COCH_3 + CO_2 + H_2O \quad (4)$$

It should be stressed that rhodium catalyst is more active than nickel catalyst as demonstrated by the higher conversion levels attained at the temperatures of 550 and 650 °C. The acetic acid conversion over Rh is higher than 70% at 550 °C while for nickel the corresponding value is 45%. The activity measurements coupled with the physicochemical characterization data indicate the different catalysts functionality that influences their reforming activity. Considering the dispersion results, the higher than Ni dispersion of Rh, contributes to the higher activity of the Rh catalyst although its loading is 10 times lower. The intrinsic activity of Rh sites is higher than that of Ni as shown from the higher TOF values at 550 °C (expressed as the moles of acetic acid converted per mole of active metal per second). With Rh the TOF is calculated at 32.6 s^{-1} while with Ni this value is 14.0 s^{-1}.

3.3. Stability test

The performance of the more active catalyst, 0.5Rh/Ce–Zr, in acetic acid reforming was further tested for extended period of time, 15 h TOS (Fig. 4). Both the conversion and the products' yield decline slightly with time due to the catalyst deactivation. After 15 h TOS a decrease of about 20% in acetic acid conversion is observed. The yield of products follows the same trend supposing the gradual decrease of the number of the accessible active sites.

3.4. Quantitative analysis of coke deposition

Carbon deposition is one of the major drawbacks for the successful realization of bio-oil reforming. For this reason the coke production rate was studied in a separate series of experiments conducted at constant temperature of 750 °C for 3 h time on stream. The used catalysts were then transferred to stoichiometric CHN analyzer for the measurement of the deposited carbon.

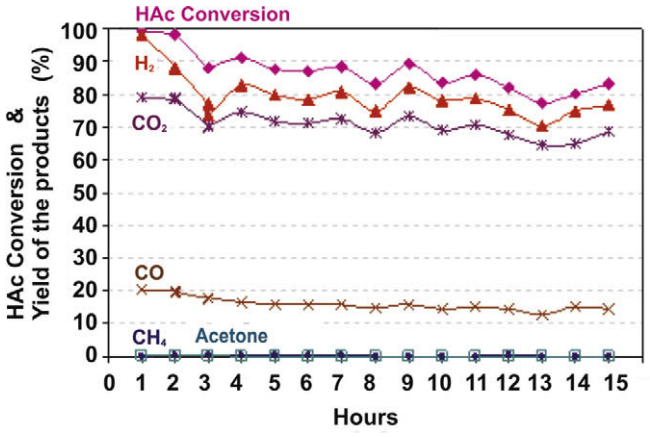

Fig. 4. Steam reforming of acetic acid over 0.5Rh/CeO_2–ZrO_2 catalyst as a function of time on stream (steam/carbon = 3, reaction temperature = 650 °C).

Table 4 presents the results of coke produced in acetic acid reforming. The amount of coke deposited is expressed as (i) wt% coke on catalyst defined as the percentage of the amount of coke produced after 3 h time on stream divided by the amount of the catalyst used and (ii) as the percentage of the C moles in the feedstock that are converted to coke.

The amount of coke measured was quite high, 4.5 wt% for the bare support indicating that mixed CeO_2–ZrO_2 favors the reactions leading to carbonaceous deposits. The high amount of the deposits on the surface of the ceria–zirconia was rather expected as high ethylene yield was detected in the gaseous stream (Table 3). Ethylene and in general olefinic compounds are considered as the precursors of carbon deposits [49–52].

The addition of nickel to CeO_2–ZrO_2 results in a reduction of deposited coke, 1.5 wt% on catalyst, either by inhibiting its formation or by facilitating the oxidation reactions. The addition of Rh as active metal almost eliminates the deposits (0.36 wt% or 0.007 mol C/mol of C in incoming HAc). The acidity of the catalysts (Table 1) does not seem to be the critical factor for carbon formation as one might expect higher deposition rates over the more acidic Rh catalysts. The present results confirm the lower affinity for carbon formation of noble metal catalysts well known from the literature [53] and the high oxygen mobility of ceria–zirconia that facilitates the surface oxidation reactions leaving the surface of the catalyst clean. Correlations of coke deposition and the oxygen mobility are elaborated in Section 3.6.

The resistance of Rh/Ce–Zr to coke deposition was also checked for longer reaction times, 15 h TOS. It was observed that the rate of reactions leading to coke does not change with time on stream as the final total amount of deposits was still very low.

3.5. Qualitative analysis of coke

Apart from the quantity of the carbon produced via the reforming process, the quality of the coke is also a substantial parameter in catalyst evaluation. Thermogravimetric analysis of the used catalysts in air flow led us to essential conclusions about the type and the location of the carbonaceous deposits.

Fig. 5 shows the results of the oxidation of the carbon deposited on the surface of the catalytic materials. The nature of the active metal determines not only the amount of coke deposited but also its nature as well, as evidenced from the profiles of the differential weight loss of the materials. It is well known that the usual graphitic or filamentous coke is burned around 500 °C [54,55] in the same range with the oxidation of the carbonaceous deposits on the surface of the 5Ni/Ce–Zr catalyst. In addition, SEM image of the used 5Ni/Ce–Zr catalyst clearly reveals that the coke deposited on the 5Ni/Ce–Zr catalyst is in the form of filamentous coke (Fig. 6). No indication of filamentous carbon was found in the images of the bare support and the 0.5Rh/Ce–Zr (not shown).

A similarity in oxidation characteristics of the carbon deposits appears with the support and the Rh catalyst. Coke deposits are oxidized at temperatures much lower than 500 °C. In the case of

Table 4
Total carbon deposits after acetic acid (HAc) steam reforming at 750 °C for 3 h.

Sample	Wt% coke on catalyst	Mol $C_{(s)}$/mol C in HAc
CeO_2–ZrO_2	4.5	0.088
5Ni/Ce–Zr	1.5	0.029
0.5Rh/Ce–Zr	0.36	0.007
0.5Rh/Ce–Zr[a]	1.71	0.007

[a] After 15 h TOS.

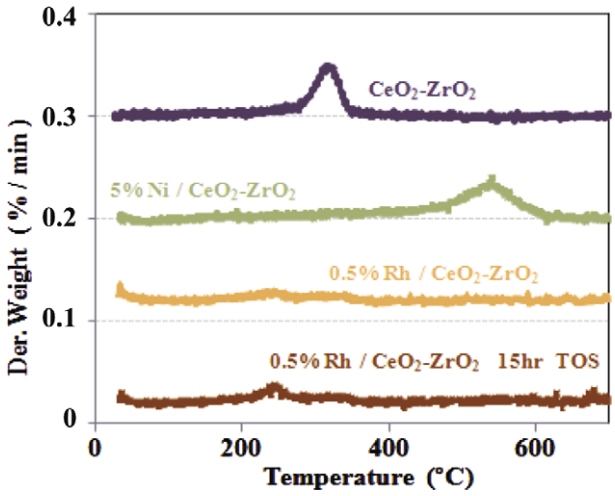

Fig. 5. Thermo gravimetric analysis of used catalysts in air flow.

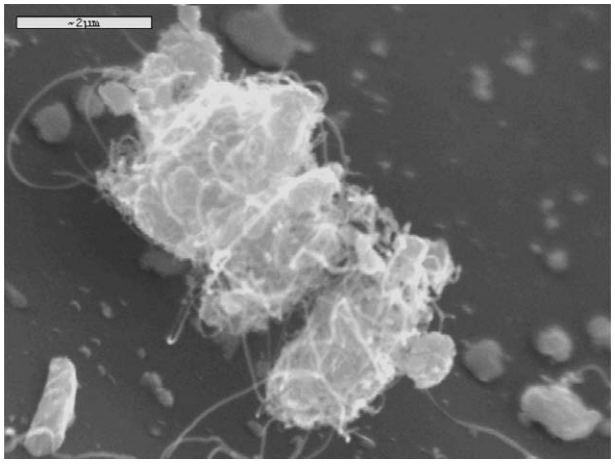

Fig. 6. Scanning electron microscopy of 5% $Ni/CeO_2–ZrO_2$ catalyst after reaction.

Rh catalyst, the onset of oxidation is at 220 °C extending up to 350 °C while for the support alone coke is mostly removed in the range of 300–350 °C. This low temperature of oxidation implies that the measured coke deposits on the surface of Ce–Zr and 0.5Rh/CeZr are not real coke but rather strongly adsorbed carbonaceous compounds–precursors of coke. According to the literature, acetic acid is adsorbed on the surface of the catalysts under reforming conditions [16]. The adsorbed molecules can lead to the formation of other more dehydrated/dehydrogenated species which are detected as easily oxidizable carbonaceous species of amorphous type [55,56]. The amorphous nature of the deposits on the surface of the used Ce–Zr and 0.5Rh/Ce–Zr is confirmed as no indication of filamentous carbon was observed in their SEM micrographs as mentioned before.

This similarity in the oxidation temperature of the carbonaceous deposits of the bare support and the Rh catalyst indirectly points that over Rh catalyst the low carbon deposits are located on the uncovered support surface and are likely the coke precursors. Besides, it has been reported that these carbonaceous deposits treated at mild conditions, called "soft" coke, do not accumulate on the active sites [57]. In the case of Ni catalysts the present results suggest that most probably carbon deposits are located on the metal crystallites with their nature being closer to that of typical coke formed during reforming of hydrocarbons and oxygenates [54,57].

In addition to the TGA profiles of the used catalysts after 3 h TOS, the corresponding profile of the used 15 h TOS 0.5Rh/Ce–Zr catalyst is presented. The oxidation profile confirms that the nature of the deposits do not change with time on stream, as the peak of its oxidation remains at low temperature.

3.6. Oxygen storage capacity (OSC)

Ceria–zirconia-mixed oxides are widely used in catalysis because of their ability to store oxygen under lean conditions (excess of oxygen) and to release oxygen under rich conditions (excess of fuel). This property, known as oxygen storage capacity (OSC), has been studied in the literature [58–63].

Present OSC measurements were conducted applying hydrogen pulses to fresh catalysts, at 750 °C. The oxygen storage capacity was measured in oxidized state and in reduced state of the catalysts simulating the conditions used in reforming reaction. In the first case, no other pretreatment of the catalysts was applied, apart from He flushing while in the second case the catalysts were pre-reduced with H_2 flow for 1 h at 750 °C.

The amount of hydrogen consumed in the first pulse and consequently that of the corresponding oxygen of the catalyst is determined as the OSC while the sum of the first 10 pulses as the OSCC. Fig. 7 depicts the results of the OSC and OSCC measurements at 750 °C with catalysts in oxidized form. The OSC (first pulse) is the same for the three samples (100 μmol/g). The amount of 100 μmol of oxygen titrated with hydrogen corresponds to 20% of the surface oxygen of CeO_2. The differentiations between Rh catalyst and the support are rather insignificant. Rh does not increase the amount of active oxygen, either the OSC or the OSCC as shown from the data in Fig. 7. Even though the literature data agree that the addition of Rh increases the OSC, present results do not support this, most probably due to the high temperature used. At such a high temperature, 750 °C, used in the present study, the differences observed are minimal. However, with the Ni-containing sample, the profile of the consumed hydrogen steepens with increasing number of hydrogen pulses. The difference is due to the removal of the oxygen associated with nickel in the form of NiO. As the amount of Ni is 5 wt%, the oxygen associated with the metal contributes substantially to the increased demand for hydrogen. It is worthy to note that with the Rh sample this difference due to the oxygen associated with Rh is not easily seen as the Rh loading is much lower, 0.5 wt%.

The results of the OSC measurements on the pre-reduced samples at 750 °C (Fig. 8) show that the OSCC or the oxygen storage after 10 pulses follows the series CeZr > 5Ni/CeZr > 0.5Rh/CeZr. The amount of oxygen that is titrated with hydrogen pulsed at

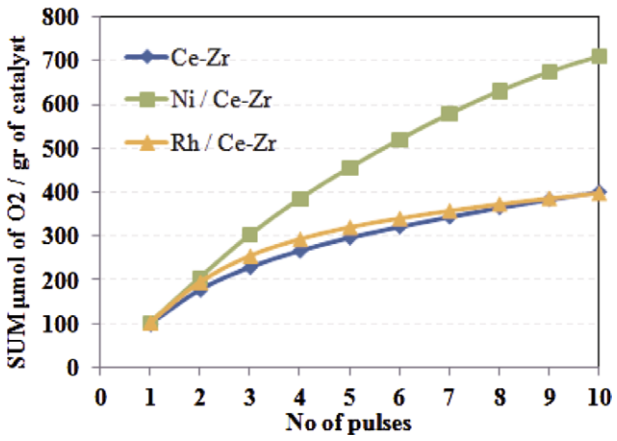

Fig. 7. Oxygen storage capacity of oxidized catalysts at 750 °C.

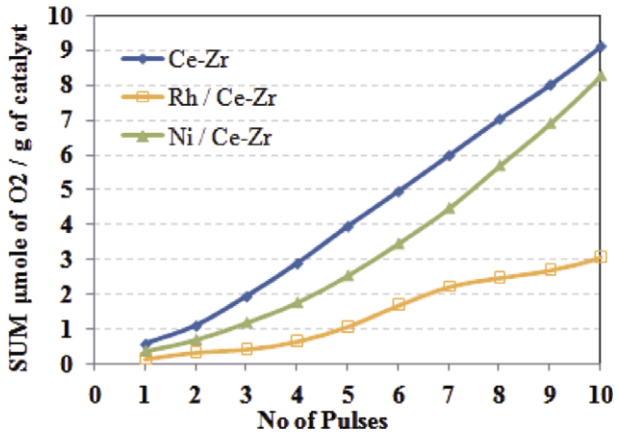

Fig. 8. Oxygen storage capacity of reduced catalysts at 750 °C.

750 °C is quite low not surpassing the 10 µmol of O_2/g of catalyst for the ceria–zirconia. The presence of the metals and especially of Rh seems to facilitate the extended reduction of the support in agreement with our TPR results and the literature data [61].

3.7. Oxygen isotopic exchange

Besides the amount of active oxygen, its mobility is of great importance for the Ce–Zr-based catalysts. A powerful technique for the determination of the oxygen mobility is the isotopic exchange with gaseous oxygen. Oxygen mobility on ceria–zirconia has been the subject of quite a few publications [40,64–67].

According to Winter [68] and Boreskov [69] there are two types of the isotopic exchange of $^{18}O_2$ between gas phase and the solid:

The simple hetero-exchange

$$^{18}O_2(g) + {}^{16}O(s) \leftrightarrow {}^{18}O(s) + {}^{16}O{}^{18}O(g)$$

and

the multiple hetero-exchange

$$^{18}O_2(g) + 2{}^{16}O(s) \leftrightarrow 2{}^{18}O(s) + {}^{16}O_2(g)$$

Temperature-programed $^{18}O_2$ isotope exchange (TPIE) measurements were conducted on the bare support and the two catalysts and the profiles of the exchanged isotopomers, $^{16}O_2$ and the cross-labeled $^{18}O^{16}O$, as a function of temperature are presented in Fig. 9a–c.

The oxygen exchange process starts at low temperature. As shown in Table 5 the onset temperature for the exchange process is around 330 °C for the Ni and Rh catalysts while for the support alone is 360 °C. The signal of $^{16}O_2$ released from the surface of all three samples dominates at the initial steps of the exchange as shown in Fig. 9a–c indicating that the multiple hetero-exchange prevails. These results are in agreement with the literature data according to which Ce–Zr-mixed oxides predominantly exchange their oxygen via a multiple exchange process, parallelizing this with the presence of binuclear oxygen species on the surface [70]. The evolution of the cross-labeled oxygen $^{16}O^{18}O$ proceeds with lower rates and becomes significant at higher temperatures suggesting the participation of the simple hetero-exchange mechanism as well. Simple calculations of the total amounts of the two isotopomers released in the gas phase up to monolayer demonstrate that at least over 85% of the exchanged oxygen is formed via the multiple hetero-exchange (Table 5). The exchange of oxygen is not limited to the external oxygen layer but is extended to the bulk as shown by the intensity of the isotopomer signals up to 750 °C (Fig. 9). However the rates of exchange are significantly lower due to the diffusion barriers from the bulk of the particles to the surface.

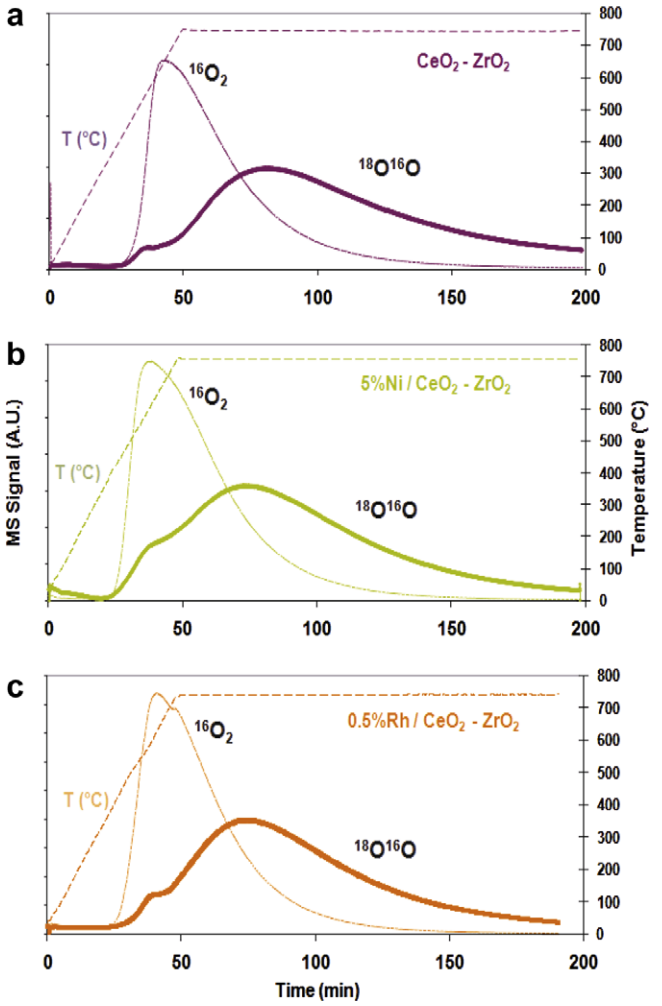

Fig. 9. Thermal programing of materials in $^{18}O_2$ flow (2% in He). Profiles of oxygen exchanged ($^{16}O_2$ and $^{18}O^{16}O$).

Table 5
Characteristics of oxygen isotopic exchange.

Sample	T_{onset} (°C)	$T_{monolayer}$ (°C)	$^{16}O_2/(^{18}O^{16}O + {}^{16}O_2)$ (up to monolayer)	Ea (kJ/mol)
CeO_2–ZrO_2	360	645	0.88	115.4
5Ni/Ce–Zr	334	490	0.85	59.2
0.5Rh/Ce–Zr	330	555	0.91	106.5

Present results do not allow for the direct calculation of the extent of oxygen exchange driven via the metallic sites to that directly driven via the support. However, it is clear that the presence of metal indeed changes the contribution of the individual steps to the total amount exchanged and the relative rates. The apparent activation energies, as calculated based on the changes of the overall exchange rate of gaseous $^{18}O_2$ with varying temperature, demonstrate that the presence of metals enhances the exchange process (Table 5) in line with the published data [66,67]. The enhancement is more clear with Ni as evidenced by the much lower activation energy which amounts to 59.2 kJ/mol compared to that of the ceria–zirconia alone, 115.4 kJ/mol.

It has been reported that a strong metal/support interaction leads to modifications in the electronic properties of the supported metals which sequentially influence the oxygen activation process [65,66]. In particular, the presence of vacancies, even in small

amounts, favors the lattice oxygen mobility. Considering the different reduction temperature applied to Ni (470 °C) and Rh (300 °C) catalysts before the isotopic exchange tests, we can conclude, in agreement with our TPR results, that in the case of Ni catalyst, a part of ceria is more likely in the reduced state. Reduced ceria as in the case of 5Ni/Ce–Zr means higher concentration of oxygen vacancies compared to that in 0.5Rh/Ce–Zr. As previously mentioned, oxygen vacancies favor the oxygen mobility resulting in this surprisingly much lower energy activation of oxygen in Ni than in Rh catalyst.

3.8. Mobility of oxygen and coking tendency in acetic acid reforming

As mentioned above the generation of oxygen vacancies is greatly affected by the reduction characteristics. According to the OSC results of the reduced at 750 °C catalysts (Fig. 8), which show that the amount of titrated oxygen of Rh catalyst is lower than that of Ni, we can conclude that with 0.5Rh/Ce–Zr catalyst the extent of reduction and consequently the number of oxygen vacancies is higher than that of Ni catalyst. This may also hold true for the reforming experiments. Under steam-reforming conditions the catalysts are in reduced state which means that oxygen vacancies are present on the surface of ceria. Even though there is no oxygen in the gas phase, water and/or even CO_2 formed can serve as oxidizing medium. Water and/or CO_2 molecules dissociate on the surface and the atomic oxygen formed reoxidizes ceria. The higher is the number of the oxygen vacant sites the higher is the mobility of this atomic oxygen which can act as oxidant for the carbonaceous deposits. It is well postulated in the literature [71–74] that the reduced ceria (CeO_{2-x}) enhances the dissociation of H_2O and CO_2. Both H_2O and CO_2 via their dissociation reaction on the surface provide active [O] to the support so as to oxidize the reduced ceria.

In the acetic acid reforming tests, the reduction conditions applied were the same (1 h at 750 °C) for the Ni catalyst, Rh catalyst, and the bare support. The latter shows relatively low reforming activity in acetic acid with relatively high selectivity to C_2 olefins and coke deposits (Table 3). It seems that the rates of reforming of the strongly adsorbed intermediate species are not high enough nor the oxygen capacity of ceria to oxidize them and leave the surface clean. That is why the amount of carbonaceous species on the bare support is quite high compared to the corresponding deposits of the other two metal-containing catalytic materials. The presence of small quantities of coke over the Ni catalyst, most probably residing on the metal crystallites, shows that at 750 °C the quantity of oxygen transferred through the support vacancies at the perimeter of the metal crystallites is not enough to fully oxidize the remaining solid carbon species. With the Rh catalysts the almost negligible carbonaceous deposition can be ascribed to the very low affinity of the metal to coking and to the rapid supply of oxygen to the metal interface.

4. Conclusions

Acetic acid reforming proceeds with high rates over Rh and Ni catalysts supported on ceria–zirconia. The activity of bare support is relatively low even at 750 °C with prevailing reactions that of decarboxylation, decomposition, steam reforming, and water gas shift. The formation of substantial amounts of C_2 hydrocarbons and especially of ethylene contributes to the relatively high deposition rate carbonaneous deposits on the surface of the mixed ceria–zirconia.

The addition of the metals enables the reforming reactions to dominate as revealed from the high hydrogen yield close to thermodynamic limits at temperature over 650 °C. The addition of metals decreases drastically the rates of coke deposition. Over Rh catalyst the deposition rate at 750 °C is 0.007 mol $C_{(s)}$/mol C of acetic acid. A similarity in oxidation characteristics of the carbon deposits appears with the bare support and the Rh catalyst. The low temperature of oxidation up to 350 °C implies that the measured coke deposits on the surface of CeO_2–ZrO_2 and 0.5Rh/CeO_2–ZrO_2 are not real coke but rather strongly adsorbed carbonaceous compounds–precursors of coke which in the case of the latter are located on the uncovered support surface. In contrast, the slightly higher coke deposits over Ni catalyst most probably residing on metal crystallites are of filamentous type oxidized at 500 °C.

The temperature-programed oxygen isotopic exchange experiments showed that the presence of metals facilitates the exchange process which proceeds up to monolayer mainly via the multiple hetero-exchange route. The rates of oxygen exchanged are much higher over the Ni catalyst as evidenced by the reduced value of the apparent activation energy. The significantly lower activation energy results from the higher extent of support reduction accompanied by increased number of oxygen vacancies which facilitate the oxygen mobility.

The presence of small quantities of coke over the Ni catalyst shows that at 750 °C the quantity of oxygen transferred through the support vacancies at the perimeter of the metal crystallites is not enough to fully oxidize the remaining solid carbon species. With the Rh catalysts the almost negligible carbonaceous deposition can be ascribed to the very low affinity of the metal to coking and to the rapid supply of oxygen to the metal interface. The loss of activity by 20% after 15 h TOS may be due to sintering of the 0.5Rh/CeO_2–ZrO_2. Further studies are in progress to improve the long-term stability of the catalyst under reforming conditions.

Acknowledgments

This research project (PENED) is co-financed by EU-European Social Fund (75%) and the Greek Ministry of Development-GSRT (25%).

References

[1] M.A. Pena, J.P. Gomez, J.L.G. Fierro, Appl. Catal. A: Gen. 144 (1996) 7–57.
[2] D. Sutton, B. Kelleher, J.R.H. Ross, Fuel Process. Technol. 73 (2001) 155–173.
[3] J. Schoeters, K. Maniatis, A. Buekens, Biomass 19 (1989) 129–143.
[4] G. Chen, J. Andries, Z. Luo, H. Spliethoff, Energy Convers. Manage. 44 (2003) 1875–1884.
[5] Z. Qi, C. Jie, W. Tiejun, X. Ying, Energy Convers. Manage. 48 (2007) 87–92.
[6] A.A. Lappas, M.C. Samolada, D.K. Iatridis, S.S. Voutetakis, I.A. Vasalos, Fuel 81 (2002) 2087–2095.
[7] J.P. Diebold, A Review of the Chemical and Physical Mechanisms of the Storage Stability of Fast Pyrolysis Bio-oils, National Renewable Energy Laboratory (NREL) Internal Report, August 26, 1999, pp. 1–51.
[8] E.Ch. Vagia, A.A. Lemonidou, Int. J. Hydrogen Energy 32 (2) (2007) 212–223.
[9] E.Ch. Vagia, A.A. Lemonidou, Int. J. Hydrogen Energy 33 (10) (2008) 2489–2500.
[10] D. Wang, D. Montane, E. Chornet, Appl. Catal. A: Gen. 143 (1996) 245–270.
[11] M. Marquevich, S. Czernik, E. Chornet, D. Montane, Energy Fuel 13 (1999) 1160–1166.
[12] P.N. Kechagiopoulos, S.S. Voutetakis, A.A. Lemonidou, I.A. Vasalos, Energy Fuel 20 (2006) 2155–2163.
[13] J.R. Galdamez, L. Garcia, R. Bilbao, Energy Fuel 19 (3) (2005) 1133–1142.
[14] F. Bimbela, M. Oliva, J. Ruiz, L. Garcia, J. Arauzo, J. Anal. Appl. Pyrol. 79 (1–2) (2007) 112–120.
[15] A.C. Basagiannis, X.E. Verykios, Int. J. Hydrogen Energy 32 (15) (2007) 3343–3355.
[16] A.C. Basagiannis, X.E. Verykios, Appl. Catal. A: Gen. 308 (2006) 182–193.
[17] A.C. Basagiannis, X.E. Verykios, Appl. Catal. B: Environ. 82 (2008) 77–88.
[18] K. Takanabe, K. Aika, K. Seshan, L. Lefferts, Chem. Eng. J. 120 (2006) 133–137.
[19] C. Rioche, S. Kulkarni, F.C. Meunier, J.P. Breen, R. Burch, Appl. Catal. B: Environ. 61 (2005) 130–139.
[20] K. Takanabe, K. Aika, K. Inazu, T. Baba, K. Seshan, L. Lefferts, J. Catal. 243 (2006) 263–269.
[21] S.A. Larrondo, A. Kodjaian, I. Fabregas, M.G. Zimicz, D.G. Lamas, B.E. Walsoe de Reca, N.E. Amadeo, Int. J. Hydrogen Energy 33 (2008) 3607–3613.
[22] S.N. Pavlova, N.N. Sazonova, J.A. Ivanova, V.A. Sadykov, O.I. Snegurenko, V.A. Rogov, I.A. Zolotarskii, E.M. Moroz, Catal. Today 91–92 (2004) 299–303.
[23] J. Chen, Q. Wu, J. Zhang, J. Zhang, Fuel 87 (2008) 2901–2907.

[24] F.B. Noronha, E.C. Fendley, R.R. Soares, W.E. Alvarez, D.E. Resasco, Chem. Eng. J. 82 (2001) 21–31.
[25] W. Wang, S.M. Stagg-Williams, F.B. Noronha, L.V. Mattos, F.B. Passos, Catal. Today 98 (2004) 553–563.
[26] T. Zhu, M. Flytzani-Stephanopoulos, Appl. Catal. A: Gen. 208 (2001) 403–417.
[27] H.-S. Roh, H.S. Potdar, K.-W. Jun, J.-W. Kim, Y.-S. Oh, Appl. Catal. A: Gen. 276 (2004) 231–239.
[28] K. Kusakabe, K.-I. Sotowa, T. Eda, Y. Iwamoto, Fuel Process. Technol. 86 (2004) 319–326.
[29] L. Rogatis, T. Montini, M.F. Casula, P. Fornasiero, J. Alloy Compd. 451 (2008) 516–520.
[30] A. Birot, F. Epron, C. Descorme, D. Duprez, Appl. Catal. B: Environ. 79 (2008) 17–25.
[31] P. Yaseneva, S. Pavlova, V. Sadykov, G. Alikina, A. Lykashevich, V. Rogov, S. Belochapkine, J. Ross, Catal. Today 137 (2008) 23–28.
[32] C. Diagne, H. Idriss, A. Kiennemann, Catal. Commun. 3 (2002) 565–571.
[33] K. Polychronopoulou, C.N. Costa, A.M. Efstathiou, Appl. Catal. A: Gen. 272 (2004) 37–52.
[34] D. Srinivas, C.V.V. Satyanarayana, H.S. Potdar, P. Ratnasamy, Appl. Catal. A: Gen. 246 (2003) 323–334.
[35] Lj. Kundakovic, M. Flytzani-Stephanopoulos, Appl. Catal. A: Gen. 171 (1998) 13–29.
[36] S. Meriani, Mater. Sci. Eng. A – Struct. 109 (1989) 121–130.
[37] M.E. Domine, E.E. Iojoiu, T. Davidian, N. Guilhaume, C. Mirodatos, Catal. Today 133–135 (2008) 565–573.
[38] C. Rioche, S. Kulkani, F.C. Meunier, J.P. Breen, R. Burch, Appl. Catal. B: Environ. 61 (2005) 144–153.
[39] E.Ch. Vagia, A.A. Lemonidou, Appl. Catal. A: Gen. 351 (1) (2008) 111–121.
[40] Y. Madier, C. Descorme, A.M. LeGovic, D. Duprez, J. Phys. Chem. B 103 (1999) 10999–11006.
[41] F. Aupretre, C. Descorme, D. Duprez, D. Casanave, D. Uzio, J. Catal. 233 (2005) 464–477.
[42] G. Lischke, B. Parlitz, U. Lohse, E. Schreier, R. Fricke, Appl. Catal. A: Gen. 166 (1998) 351–361.
[43] P. Biswas, D. Kunzru, Int. J. Hydrogen Energy 32 (2007) 969–980.
[44] D. Michel, F. Faudot, E. Gaffet, L. Mazerolles, J. Am. Ceram. Soc. 76 (1993) 2884–2888.
[45] N. Liu, Z. Yuan, C. Wang, S. Wang, C. Zhang, S. Wang, Fuel Process. Technol. 89 (2008) 574–581.
[46] J. Kaspar, P. Fornasiero, M. Graziani, Catal. Today 50 (1999) 285–298.
[47] W.-S. Dong, H.-S. Roh, K.-W. Jun, S.-E. Park, Y.-S. Oh, Appl. Catal. A: Gen. 226 (2002) 63–72.
[48] S. Eriksson, A. Schneider, J. Mantzaras, M. Wolf, S. Jaras, Chem. Eng. Sci. 62 (2007) 3991–4011.
[49] F. Aupretre, C. Descorme, D. Duprez, D. Casanave, D. Uzio, J. Catal. 233 (2) (2005) 464–477.
[50] J.R. Rostrup-Nielsen, Catal. Today 18 (1993) 305–324.
[51] M. Virginie, M. Araque, A.C. Roger, J.C. Vargas, A. Kiennemann, Catal. Today 138 (2008) 21–27.
[52] F. Romero-Sarria, J.C. Vargas, A.C. Roger, A. Kiennemann, Catal. Today 133–135 (2008) 149–153.
[53] J.R. Rostrup-Nielsen, in: J.R. Anderson, M.J. Boudart (Eds.), Catalysis, Science and Technology, Springer Verlag, 1984.
[54] M.C. Sanchez-Sanchez, R.M. Navarro, J.L.G. Fierro, Int. J. Hydrogen Energy 32 (2007) 1462–1471.
[55] J. Guo, H. Lou, H. Zhao, D. Chai, X. Zheng, Appl. Catal. A: Gen. 273 (2004) 75–82.
[56] K.Y. Koo, H.-S. Roh, Y.T. Seo, D.J. Seo, W.L. Yoon, S.B. Park, Appl. Catal. A: Gen. 340 (2008) 183–190.
[57] A. Shamsi, J.J. Spivey, J.P. Baltrus, Appl. Catal. A: Gen. 293 (2005) 145–152.
[58] J. Fan, X. Wu, Q. Liang, R. Ran, D. Weng, Appl. Catal. B: Environ. 81 (2008) 38–48.
[59] W. Xiaodong, L. Qing, W. Xiaodi, W. Duan, J. Rare Earth 25 (2007) 416–421.
[60] Z. Zengzan, L. Bing, Z. Aimin, L. Jun, Z. Yunkun, J. Rare Earth 24 (2006) 35.
[61] J.-R. Kim, W.-J. Myeong, S.-K. Ihm, Appl. Catal. B: Environ. 71 (2007) 57–63.
[62] L. Kai, W. Xuezhong, Z. Zexing, W. Xiaodong, W. Duan, J. Rare Earth 25 (2007) 6–10.
[63] Z. Zengzan, L. Bing, Z. Aimin, L. Jun, Z. Yunkun, J. Rare Earth 24 (2006) 35–38.
[64] P. Fornasiero, R. Monte, G.R. Rao, J. Kaspar, S. Meriani, A. Trovarelli, M. Graziani, J. Catal. 151 (1995) 168–177.
[65] S. Bedrane, C. Descorme, D. Duprez, Appl. Catal. A: Gen. 289 (2005) 90–96.
[66] C. Bozo, N. Guilhaume, J.-M. Herrmanny, J. Catal. 203 (2001) 393–406.
[67] X. Wu, J.F. RuiRan, D. Weng, Chem. Eng. 109 (2005) 133–139.
[68] E.R.S. Winter, J. Chem. Soc. 12 (1968) 2889–2902.
[69] G.K. Boreskov, Discuss. Faraday Soc. 41 (1966) 263–276.
[70] D. Duprez, C. Descorme, T. Birchem, E. Rohart Top. Catal. 16/17 (1–4) (2001) 49–56.
[71] K.Y. Koo, H.S. Roh, U.H. Jung, W.L. Yoon, Catal. Lett. 130 (2009) 217–221.
[72] K.W. Jun, H.S. Roh, K.V.R. Chary, Catal. Surv. Asia 11 (2007) 97–113.
[73] T.J. Huang, H.J. Lin, T.C. Yu, Catal. Lett. 105 (3–4) (2005) 239–247.
[74] N. Laosiripojana, S. Assabumrungrat, Appl. Catal. A: Gen. 290 (2005) 200–211.